ELSEVIER

Journal of Hazardous Materials 54 (1997) 65–87

JOURNAL OF HAZARDOUS MATERIALS

Air emissions from exposed, contaminated sediments and dredged materials 1. Experimental data in laboratory microcosms and mathematical modelling

K.T. Valsaraj [a,*], B. Choy [a,b], R. Ravikrishna [a], D.D. Reible [a], L.J. Thibodeaux [a], C.B. Price [c], J.M. Brannon [c], T.E. Myers [c]

[a] *Department of Chemical Engineering, Louisiana State University, Baton Rouge, LA 70803, USA*
[b] *Department of Chemical Engineering, University of Sydney, Sydney, Australia*
[c] *Environmental Laboratory, US Army Engineer Waterways Experiment Station, 3909 Halls Ferry Road, Vicksburg, MS 39180, USA*

Received 17 August 1996; accepted 31 October 1996

Abstract

The air emissions of two polycyclic aromatic hydrocarbons (pyrene and phenanthrene) and one heterocyclic compound (dibenzofuran) from an 'aged' contaminated sediment (Rouge River, Michigan) were studied in an experimental microcosm. The sediment-to-air flux of the above semivolatile organic compounds (SOCs) was obtained from an initially water-saturated sediment. The magnitude of flux varied as dibenzofuran > phenanthrene > pyrene. At a low air flow rate (10 ml min^{-1}) the flux was low and stable and air-phase resistance controlled. At a larger flow rate (100 ml min^{-1}) the flux was high initially and then declined, indicating the effects of sediment-side diffusion on mass transfer to air. The flux was also sensitive to the relative humidity (RH) of the air flowing above the sediment. It was observed that the flux, though high initially, declined rapidly as dry air (0% RH) was passed over the wet sediment. Loss of sediment moisture which increased the sorptive capacity of the sediment for the contaminants was also noted. Subsequent exposure of the dry sediment to humid air increased the flux. The steady state flux was consistently high when humid air was passed over dry sediment. The experimental data were analyzed using a mathematical model which estimated the air emission from an exposed sediment layer under both sediment-side and air-side resistance controlled conditions. The model incorporated an advancing 'drying front' in the direction of airflow for water evaporation in accordance

* Corresponding author. Tel.: + 1-504-3881426; fax: + 1-504-3881476; e-mail: kvalsar@lsuvm.sncc.lsu.edu.

PII S0304-3894(96)01872-9

with our observations. The sharp decrease in contaminant flux was attributed to the drying-out of the sediment and a consequent increase in its sorptive capacity for the contaminant. The framework of the theory underlying the air emission modelling from exposed sediment, dredged and placed in a confined disposal facility (CDF) is summarized. © 1997 Elsevier Science B.V.

1. Introduction

Contaminated sediments pose significant environmental problems in the United States. Almost a quarter of all Superfund National Priority List sites include contaminated sediments. Contaminants in these sediments include a number of organic and inorganic compounds. The US Army Corps of Engineers has the primary responsibility for dredging and disposal of contaminated sediments. During dredging and storage in confined disposal facilities (CDFs), there is ample opportunity for emissions of organic compounds (volatile and semi-volatile) from contaminated sediments and dredged materials. Sediments from Waukegan Harbor (Wisconsin), Indiana Harbor (Indiana), New Bedford Harbor (Massachusetts), Rouge River (Michigan) and Chicago River (Illinois) contain several organics that may be released to the air during and after disposal operations. In a recent article Valsaraj et al. [1] enumerated the possible pathways for air emissions from CDFs. The dredged material (i.e., former bed-sediment) exposed directly to the atmosphere was noted to be the major contaminant transfer locale based on the magnitudes of the areal extent, concentration of the pollutant and the mass transfer coefficient. Preliminary mathematical models to estimate these air emission rates were proposed. These models remain largely untested due to a lack of experimental data. Such vignette models are a necessary prelude to estimating risk from the air pathway exposure to contaminated sediments at low tide and dredged materials placed on-shore and developing strategies for controlling these air emissions.

After sediments are placed in a CDF, water loss by evaporation and drainage occurs. Atmospheric precipitation (rain, dew, fog) and tidal variations can then increase the sediment moisture. Sediments stored in CDFs thus go through cycles of dry and wet conditions. They are also subject to variations in air relative humidity and temperature. The sorptive capacity of a sediment is a strong function of moisture content [2]. Dry sediments generally have high adsorptive capacity for hydrophobic organic compounds. As the sediment moisture content or air relative humidity increases, the water molecules effectively displace the hydrophobic compounds from the surface and thus decrease the sediment sorptive capacity. The organic vapor concentration above contaminated sediments is influenced by the sediment moisture content, temperature and air relative humidity. Early investigations on soils showed a distinct increase in the vapor concentrations of several pesticides over water-saturated soils compared to dry soils [3]. Other work on soils included data on partitioning of several organics between air and soils of different types and the effects of relative humidity fluctuation on the emission of volatile organics [4–7,26,30]. It has been observed in the laboratory that for a sample of Indiana Harbor sediment exposed to air, an 83% reduction in total Aroclor 1248 (a mixture of several congeners of polychlorinated biphenyls) occurred in 6 months [21]. Recent work showed similar behavior for Aroclor 1242 from New Bedford Harbor, Massachusetts

sediment [8,9]. It became evident that detailed and controlled experiments were necessary, especially on semi-volatile organics to accurately assess volatilization from dry, damp and wet sediments.

The experiments described in this paper were undertaken to study the release of semivolatile organic compounds (SOCs) from an initially wet (water-saturated) sediment over which air of varying relative humidities is passed continuously to simulate conditions that might exist in a typical CDF during cyclic wet and dry periods. Experimental microcosms were used to obtain the fluxes of two polycyclic aromatic hydrocarbons (pyrene and phenanthrene) and one heterocyclic aromatic compound (dibenzofuran) from a naturally aged contaminated sediment (Rouge River, Michigan). The sediment depth used in the microcosms was very small (ca. 0.4 cm) since it provides the advantage of clearly defining the dynamic between the 'wet' and 'dry' states of the sediment and the consequent differences in the contaminant flux. This paper presents and discusses the experimental data. A framework of the theory of air emissions from an exposed sediment and a predictive mathematical model are suggested to simulate the experimental data. These efforts should prove useful in assisting the decision-making process on siting and managing contaminated sediment disposal facilities.

2. Experimental

2.1. Sediment

The sediment used in this work was obtained from the Rouge River, Michigan. Rouge River is located in the southeastern part of Michigan and empties into Lake Erie. The sediment was collected and supplied to us by the Natural Resources Research Institute, Coleraine, Minnesota. The sediment was sieved through a standard mesh (45 mm screen) upon collection and shipped to our laboratory at LSU. It was then coarse sieved (3/8 in. mesh), fine sieved (1.41 mm openings) and stored in closed plastic containers at ambient temperature in our laboratory. The properties of the sediment are given in Table 1.

Table 1
Properties of the rouge river sediment

Property	Value
Particle density, ρ_p	2.2 g cm^{-3}
Bulk density, ρ_b	0.67 g cm^{-3}
Porosity (total), ϵ_T	0.7
Overall organic carbon fraction, f_{oc}	0.08
Oil and grease fraction, f_{og}	0.04
Percent sand	60
Percent silt	36
Percent clay	3.2

Table 2
Physical and chemical properties of contaminants in the rouge river sediment [a]

Property	DBF	PHE	PYR
Sediment loading [b] (mg kg^{-1})	40 ± 7	21 ± 2	36 ± 3
Water solubility (mg l^{-1})	10	1	0.15
$\log K_{oc}$ (l kg^{-1})	4.0	4.4	4.8
$\log K_{ow}$	4.1	4.5	5.1
Henry's constant, H_c (dimensionless) [20]	3.1×10^{-3}	2.5×10^{-3}	4.5×10^{-4}
Air diffusivity (cm^2 s^{-1})	0.060	0.058	0.054
Vapor pressure (mm Hg)	3.6×10^{-3}	2.5×10^{-4}	4.5×10^{-6}
$\log K^*_{dw}$ (l kg^{-1})	5.38	5.90	7.05
$\log K^*_{dd}$ [c] (l kg^{-1})	6.8	9.0	12.6

[a] From reference [14] except where noted.
[b] From reference [16].
[c] Estimated as described in text.

2.2. Contaminants

The Rouge River sediment is contaminated with several polycyclic aromatic hydrocarbons (PAHs) and other compounds. It contains appreciable amounts of oil and grease ($f_{og} \approx 0.04$), the composition of which has not been identified. The overall total organic carbon fraction of the sediment was 0.08. We focussed only on two polycyclic aromatic hydrocarbons (pyrene, PYR, and phenanthrene, PHE) and one heterocyclic aromatic compound (dibenzofuran, DBF). The average sediment concentrations of the pollutants are given in Table 2, along with their relevant physicochemical properties. The pollutants considered have low vapor pressures, low aqueous solubilities, and high hydrophobicities (large octanol–water partition constant, $\log K_{ow}$).

2.3. Microcosms

10 microcosms were used in unison to give adequate surface area to attain detectable levels of hydrocarbons on the trapping material. Fig. 1 shows the sketch of one microcosm, the design of which is a modification of the one used by Spencer et al. [3]. The chamber was constructed of 1-in. anodized aluminum blocks, 30 cm long by 9 cm wide. The lower block contained a well 10 cm long by 3 cm wide by 2 cm deep which contained the sediment. A spacer placed in the well allowed adjustment of sediment depth to any required value. The sediment surface area was 30 cm^2 in each cell. Approximately 0.2 cm air space was left above the sediment in each cell. The upper block contained a 10 cm long by 3 cm wide hole lined on the bottom with a quartz glass sheet 0.32 cm thick. The air space was 10 cm in the direction of airflow, and also extended 5 cm on each side of the chamber. The upper block is grooved to give a 0.2 cm air space above the sediment placed in the well to allow laminar air flow. Three typical air flow rates were used in these experiments, namely, 10, 100 and 1000 cm^3 min^{-1} with corresponding air velocities ranging from 0.28 to 28 cm s^{-1} across the sediment surface.

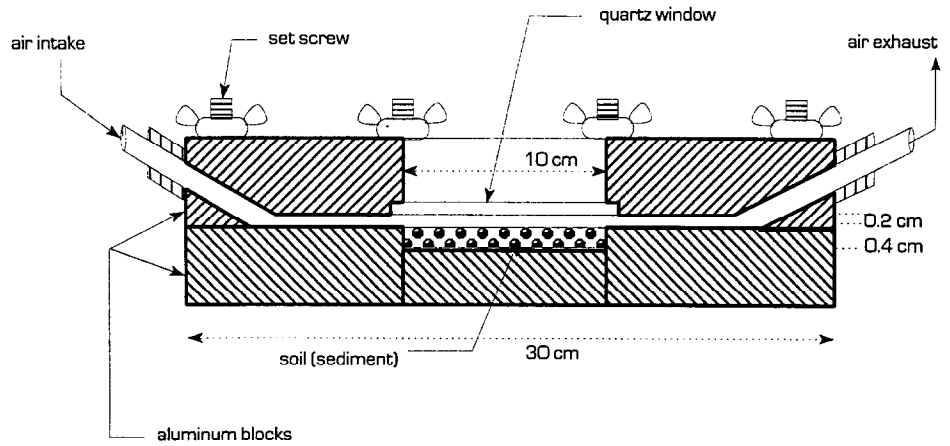

Fig. 1. Schematic of an experimental microcosm.

2.4. Determination of flux

Approximately 18 g of wet sediment (ca. 4 mm depth) was loaded into each microcosm. The sediment was spread out using a spatula. The upper block was carefully placed over it and sealed by means of a rubber O-ring and wing-nut bolts. Each chamber was equipped with a separate Gilmont flowmeter attached to a compressed air cylinder to standardize flow rate equally among the chambers. Attached to each chamber was a 11.4 cm long and 0.32 cm inside diameter stainless steel tube packed with 150 mg of Florisil. Glass wool was used to hold the trapping material inside the tubes. Air was passed over the sediment in the chambers at the required flowrate. The relative humidity of the air was controlled in some tests by bubbling it through a water trap at different flowrates and measuring the relative humidity in-line with a Tri-Sense temperature–humidity–air velocity meter and relative humidity–temperature probe (Cole Parmer, Niles, IL). The Florisil trap was changed periodically and replaced with a fresh tube to collect samples of desired duration. The Florisil samples were immediately extracted using 10 ml of a 50% methylene chloride–46% hexane–4% acetonitrile mixture and the samples from all 10 microcosms were combined to get a composite sample which was reduced in volume to 10 ml using nitrogen blowdown. Samples were placed in 20 ml amber glass bottles with teflon-lined caps and refrigerated at 4°C until analysis. Final moisture determinations were performed by consolidating the sediment from all the chambers and drying subsamples at 105°C for 24 h. Intermediate moistures were determined by sacrificing a chamber after the required time interval.

The total mass of each compound in the sample was obtained as described in the next section. The flux $N(t)$ in g cm^{-2} h^{-1} was obtained from the expression

$$N(t) = \frac{\Delta m}{\Delta t A_c} \tag{1}$$

where Δm is the mass of chemical collected in time Δt. A_c is the total sediment-air interface area in the microcosms ($= 300$ cm^2).

2.5. Analysis of compounds

The polycyclic aromatic hydrocarbons (PYR, PHE) and the heterocyclic aromatic compound (DBF) were analyzed using standard EPA method 8310 [13]. The samples were reduced further to a volume of 2 ml using ultrapure nitrogen blowdown. They were then solvent exchanged with acetonitrile. The resulting acetonitrile samples were then injected into a high pressure liquid chromatograph (Hewlett Packard Model 1090L) equipped with a variable wavelength UV detector and analyzed for the PAHs. The column used was Envirosep-PP by Phenomenex. The solvent used was a mixture of acetonitrile and water. A gradient method was used with an initial 60/40 ratio of acetonitrile/water changing to pure acetonitrile over 30 min. Concentrations were determined by comparing with standard calibrations.

3. Results and discussion

3.1. Sediment drying behavior in the experimental microcosms

The evaporation of water from soils, sediments and other porous media is a well-researched topic. Air blown across the sediment surface will remove water by evaporation. This is termed 'cross-circulation drying' [29]. The process is dependent primarily on the air flow rate, temperature and air relative humidity. In a thin layer of sediment such as the one employed in this work the evaporation of water proceeded as follows: With time as water evaporated from the sediment, a distinct 'dry' zone developed near the air inlet which was clearly separated from the remaining 'wet' zone of the sediment. This 'drying front' moved at a constant velocity in the direction of air flow across the sediment until the entire surface sediment appeared dry. Fig. 2 is a

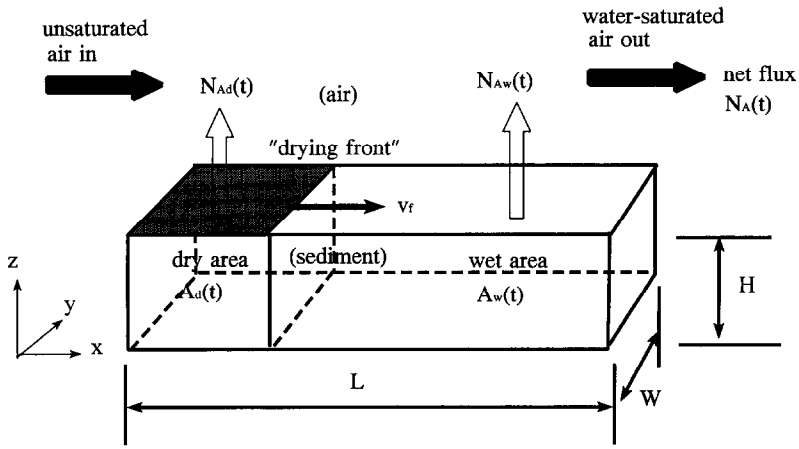

Fig. 2. A schematic of the advancing 'drying front' in a typical experiment.

schematic of this behavior in a typical experiment. The nature of the front indicated that the sediment was drying uniformly in the z-direction, and it moved across the sediment (x-direction) in much the same way as an 'adsorption wave' through a bed of carbon [11]. This behavior is a result of the small sediment depth and the low air flow velocity. These observations suggested that the overall contaminant flux, $N_A(t)$ will be the integral average over the respective areas. The ratio of the velocity of air in soil to that of the chemical vapor in soil is defined as the retardation factor. The larger the retardation factor the slower is the movement of the chemical in the soil pore space. As will be shown in a subsequent section, the retardation factor for the contaminant will be higher in the 'dry' zone as compared to the 'wet' zone of the sediment. Therefore, the contaminant flux from the dry area, $N_{Ad}(t)$ will be small, while that from the wet area, $N_{Aw}(t)$ will remain high. We thus have the contaminant flux varying from a completely wet sediment initially to a dry sediment after the 'drying front' has passed through. As the drying front advances, the overall contaminant flux will decrease. If we assume that the fluxes from the two zones are independent of one another, the vapor concentrations are small and that there is no back pressure to reduce the flux from either zone, the average contaminant flux is given by

$$N_A(t) = N_{Ad}(t)\frac{A_d(t)}{A_T} + N_{Aw}(t)\frac{A_w(t)}{A_T} \tag{2}$$

The above assumption holds since the changes in the sediment loading are relatively small ($< 3\%$) and hence the vertical profiles will not be that different across the 10 cm microcosm. The two areas, viz., the dry zone area, $A_d(t)$ and the wet zone area, $A_w(t)$ are related to the velocity (v_f) of the advancing 'drying front'. The latter is given by

$$v_f = \frac{dx}{dt} = \frac{L}{\tau_{evap}} \tag{3}$$

where L is the total length of the microcosm and τ_{evap} is the total time for evaporation of unbound water from the sediment.

$$\tau_{evap} = \frac{\gamma_0 w_s RT}{q p_w^0 M_w} \tag{4}$$

where w_s is the mass of sediment used (g) and γ_0 is the initial water content in the sediment (g g^{-1}). p_w^0 is the vapor pressure of water (atm) at temperature T and q is the air flow rate (cm^3 s^{-1}). Eq. (4) was obtained from a water mass balance assuming that the air exiting the microcosm was saturated with water vapor. Experimental demonstration of this fact is shown in Fig. 3. Fig. 3 shows the water flux (otherwise called the 'drying-rate' curve) and relative humidity of the exiting air in an experiment in which a sample of Rouge River sediment containing 53% moisture was dried by passing 0% RH air. The relative humidity (RH) of the exiting air was 100% and the water flux remained constant for a period of 44 h which is termed the 'constant-rate period'. During this period the unbound water was removed. Following this is a steep decline in water flux which is termed the 'falling-rate period'. The time for the 'drying front' to move

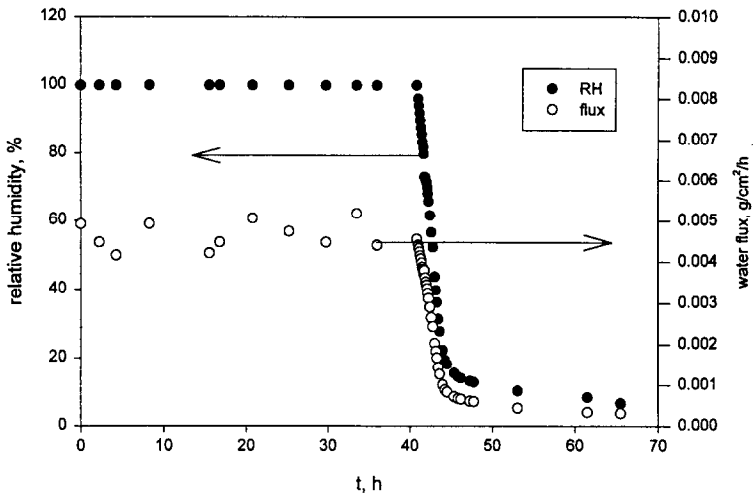

Fig. 3. The flux of water and the relative humidity of the exiting air from the microcosm. The sediment in this case had an initial water content of 53% (w/w).

through the sediment surface was the same as the 'constant-rate period'. The implication was that as dry air moved across the 'wet' zone of the sediment, water-saturation of air occurred over a thin segment of the surface sediment. Incidentally, Eq. (4) predicted a τ_{evap} of 52 h from a sediment containing 53% moisture. During the 'falling-rate' period, both the RH and the water flux decreased rapidly as the residual moisture (bound water) was removed. Solving Eq. (3) for x gives

$$x = \frac{L}{\tau_{evap}} t \tag{5}$$

Hence

$$\frac{A_d(t)}{A_T} = \frac{t}{\tau_{evap}}; \quad \frac{A_w(t)}{A_T} = 1 - \frac{t}{\tau_{evap}} \tag{6}$$

The overall contaminant flux from the sediment for $t < \tau_{evap}$ is given by

$$N_A(t) = N_{Ad}(t)\frac{t}{\tau_{evap}} + N_{Aw}(t)\left(1 - \frac{t}{\tau_{evap}}\right) \tag{7}$$

For $t \geq \tau_{evap}$, $N_A(t) = N_{ad}(t)$. For the experiments reported in this work, the initial sediment moisture content was 0.2 and hence τ_{evap} was 31 h. The above model is purely predictive in that there are no adjustable parameters involved. All the necessary key parameters for the determination of fluxes from the two zones are available from expressions as described in the following section.

3.2. Air emission flux from exposed 'wet' and 'dry' sediments

In this section, we define the equations and parameters necessary to calculate the flux from the two zones, 'wet' and 'dry'. As per our earlier work [27], we define a 'wet' sediment as one in which the water content is $> 4\%$ (w/w) and a 'dry' sediment as one in which the moisture content is $< 1\%$ (w/w). The intermediate case of 'damp' sediment is one in which the moisture content is between 1% and 4% (w/w).

Let us consider the diffusion of a compound A from an initially 'wet' or 'water-saturated' sediment across the surface of which dry air is passed. This represents the conditions existing when a water-saturated contaminated sediment is freshly dredged and placed in a CDF. The sediment quickly undergoes evaporative drying. The emission pathway for chemicals involves several steps: desorption from sediment particles into a thin film of water surrounding the particles in porewater, diffusion through the water film, desorption from the water film into the air boundary layer, and vapor phase diffusion through the air boundary layer. For compounds emerging from within soil pore spaces, there is an additional process, namely, the diffusion through the air-filled soil pores before emerging into the atmospheric boundary layer. This last step is apparently the rate controlling step on the sediment side of the interface [17]. Vapor diffusion through the air boundary layer provides the second resistance to mass transfer.

Consider a layer of 'wet' (water-saturated) sediment of depth H (cm) placed in the laboratory microcosm over which uncontaminated air is passed (Fig. 3). For this problem the diffusion equation for component A within the sediment pore spaces is given by [10]

$$\frac{\partial \rho_A}{\partial t} = \frac{D_e}{R_F} \frac{\partial^2 \rho_A}{\partial z^2} \tag{8}$$

where ρ_A is the mass concentration of chemical in sediment pore spaces (ng cm^{-3}). R_F is the retardation factor. For a 'wet' sediment it is given by $R_{Fw} = \epsilon_a + \epsilon_w/H_c + \rho_b K^*_{dw}$. K^*_{dw} is the 'wet' sediment–air partition constant for A (cm^3 g^{-1}), D_e is the effective diffusivity of A through air-filled pores as given by the Millington–Quirk expression ($= D_A \epsilon_a^{10/3}/\epsilon_T^2$) (cm^2 s^{-1}), D_A is the chemical diffusivity in air (cm^2 s^{-1}), ρ_b is the sediment bulk density (g cm^{-3}), ϵ_a is the air-filled porosity of the sediment ($= (1 - \theta)\epsilon_T$) (cm^3 cm^{-3}), ϵ_w is the water-filled porosity of the sediment ($= \theta\epsilon_T$) (cm^3 cm^{-3}), and θ is the volumetric water content in the sediment (cm^3 cm^{-3}). ϵ_T is the total porosity of the sediment (cm^3 cm^{-3}). H_c is the dimensionless Henry's constant for partitioning of chemical A between the air and aqueous phases (mass concentration ratio). z is the distance upward from the bottom of the microcosm.

For the experimental conditions of finite sediment depth, two appropriate boundary conditions and an initial condition are chosen:

(i) at $z = 0$, $\partial \rho_A/\partial z = 0$

(ii) at $z = H$, $D_e \partial \rho_A/\partial z + k_a(\rho_A - \rho_A^\infty) = 0$

(iii) at $t = 0$, $\rho_A(z,0) = \rho_A^0$ for all $z \in [0,H]$

The first boundary condition states that there is no flux at the bottom of the microcosm. The second boundary condition arises from the fact that there is an air-side resistance to

mass transfer. k_a is the air-phase boundary layer mass transfer coefficient and ρ_A^∞ is the concentration of A in the background air which is taken to be zero. The third statement is the initial condition that a uniform initial concentration of A exists within the sediment. The solution for the analogous heat conduction problem is available in the literature [23,25].

The flux of chemical at the sediment–air interface of the 'wet' sediment is then given by

$$N_{Aw}(t) = 2D_e \rho_A^0 \frac{L^2}{H} \sum_{n=1}^{\infty} \frac{\exp(-\alpha_n^2 T)}{L(L+1)+\alpha_n^2} \tag{9}$$

where $L = k_a H / D_e$; $T = D_e t / R_{Fw} H^2$. α_n are positive eigen values of the equation $\alpha_n \tan(\alpha_n) = L$. ρ_A^0 is given by w_A^0 / R_{Fw}, where w_A^0 is the initial mass of contaminant in the sediment (ng g^{-1}).

At short times no concentration gradient exists within the sediment and hence the air-side resistance controls the mass transfer. Initially ($t \approx 0$) the flux is given by $N_{Aw}(t) = k_a(\rho_A^0 - \rho_A^\infty)$. As $t \to \infty$, the flux will be dominated by the sediment-side diffusion of A. Also, as $k_a \to \infty$, the process will become entirely sediment-side diffusion controlled. It is also true that the time it takes for the process to become sediment-side diffusion controlled will be longer as R_{Fw} (or K_{dw}^*) increases. It may seem counter-intuitive at first glance that a compound more sorbing to the sediment would be more likely to be air-side controlled. Consider two chemicals with the same pore space concentration, but with different K_{dw}^*. The mass of chemical in the system will be larger for the one with larger K_{dw}^*. Thus, it will take a longer time to deplete this chemical from the sediment and therefore the build-up of sediment-side diffusion resistance for the compound will take longer.

For a 'dry' sediment, $\epsilon_w = 0$, $\epsilon_a = \epsilon_T$, $D_e = D_A \epsilon_a^{4/3}$, and hence the retardation factor is given by

$$R_{Fd} = \epsilon_a + \rho_b K_{dd}^*$$

The flux from a dry sediment, $N_{Ad}(t)$ is also given by Eq. (9) where we now have to replace $\rho_A^0 = w_A^0 / R_{Fd}$, $L = k_a H / D_e$; $T = D_e t / R_{Fd} H^2$.

The main point of the above discussion is that on the sediment-side of the interface the ratio D_e / R_F determines the magnitude of the air emission flux from both 'wet' and 'dry' sediments. On the air-side of the interface the mass transfer coefficient k_a controls the air emission rate. D_e is a function of sediment moisture content. R_F is a strong function of sediment moisture content through its dependence on K_d^*. k_a is primarily dependent on the air velocity. These parameters were calculated from the equations described below.

3.2.1. Effective diffusivity

As described earlier, the effective diffusivity is that given by the Millington–Quirk expression [28]. Evidently the effective diffusivity, D_e, changes from a large value for the 'dry' sediment to progressively smaller values as the sediment moisture content increases, since the importance of the vapor-phase pathway diminishes, while the aqueous-phase pathway increases [10,15].

3.2.2. Sediment / air partition coefficient

The sediment-to-air partition constant, K_d^* in the above equations is the ratio of the equilibrium concentration of A on the sediment (w_A^* in ng g^{-1}) to the vapor concentration of A (C_a^* in ng cm^{-3}).

$$K_d^* = \frac{w_A^*}{C_a^*} \tag{11}$$

The partition coefficient takes on different values depending on the sediment moisture content and air relative humidity.

For a water-saturated wet sediment $K_{dw}^* = K_{oc} f_{oc} / H_c$, where K_{oc} is the organic carbon based sediment–water partition constant for chemical A (cm^3 g^{-1}) and f_{oc} is the fraction organic carbon in the sediment. Since the Rouge River sediment contains ca. 4% oil and grease besides sedimentary organic carbon, the pollutants can partition into both phases. f_{oc} represents the overall organic carbon content, which was 0.08 in this case. H_c is the Henry's constant which is the ratio of molar concentrations in air to water. Values of K_{dw}^* for the 'wet' sediment case are given in Table 2 for DBF, PHE and PYR. These were obtained from actual experimental values of K_{oc} determined previously in our laboratory [14].

An air-dry sediment has a large binding capacity for most hydrophobic organic compounds, and hence shows a large K_{dd}^* value. As sediment moisture content or air relative humidity increases, water molecules effectively compete for adsorption sites on the sediment solids and therefore the value of K_{dd}^* for most organics show small values at high moisture levels [11]. The value of K_{dd}^* for a 'dry' sediment is given by $w_A^m B_A / C_A^0$ [11]. The value of w_A^m, the concentration of A required for a monolayer coverage on the sediment is given by $0.917\, f S_a (d_A^2 M_A / N)^{1/3}$, where f is the fraction of the total sediment surface area (S_a) available for adsorption, d_A is the density of the compound A, M_A is the molecular weight of A and N is the Avogadro number. C_A^0 is the saturated vapor concentration (molar) of compound A in air. A typical value of the BET isotherm parameter, $B_A = 80$ can be used [2]. The total surface area of the sediment S_a can be estimated from the individual contributions of its components $\sum_i^n a_{mi} \phi_i$, where a_{mi} is the total surface area of component i and ϕ_i denotes the mass fraction of component i [10]. The value so calculated for Rouge River sediment was 93 m^2 g^{-1}. Values of K_d^* for the dry sediment are presented in Table 2. Owing to the unfortunate lack of data on K_d^* for these compounds on dry soils or sediments, this is the best available estimate at present. It is important, however, to note that the values of K_{dd}^* are several orders of magnitude greater than K_{dw}^* for the three compounds.

3.2.3. Air-side mass transfer coefficient

The value of the air-side mass transfer coefficient k_a is known to a lesser extent, although some expressions are available in the literature [12]. Table 1 lists two expressions obtained from penetration theory and boundary layer approaches. In both expressions k_a is related to the air velocity across the sediment surface, and compound properties (e.g., diffusivity in air). The value of k_a increases as the square root of the air velocity; the larger the k_a value, the smaller is the air-side resistance to mass transfer.

3.3. Experimental results in laboratory microcosms

Several experiments were conducted to obtain the sediment-to-air fluxes of two polyaromatic hydrocarbons (PHE and PYR) and one heterocyclic compound (DBF) from contaminated Rouge River sediment. DBF has the highest vapor pressure and Henry's constant whereas, PYR has the lowest vapor pressure and Henry's constant. The sediment–air partition constant K_d^* for a wet sediment varied as DBF < PYR. Fig. 4 shows the flux of DBF from an initially wet sediment (20% w/w moisture content) over the surface of which dry air (zero relative humidity) at 100 ml min^{-1} was passed through for 144 h. Each data point in the figure is an average of 5 replicate experiments. The first sample was collected after 2 h at which a high flux (60 ng cm^{-2} h^{-1}) with a large standard error was obtained. The standard error was smaller for the subsequent data points as seen from Fig. 4. Within about 30 h the flux decreased rapidly and reached a steady state value of ca. 0.2 ng cm^{-2} h^{-1} towards the end of the run. As volatilization from the sediment continues, the top layer becomes quickly depleted of DBF. Further, losses will then come via diffusion of DBF from within sediment pore spaces. It was observed that the wet sediment (20% w/w initial moisture content) quickly lost moisture (0.67% w/w final moisture content) as dry air was passed over it for 72 h. Decreased moisture in the air means loss of water from the sediment to air which may result in the transport of water from the deeper sediment layers to the surface which carries with it some organics which volatilize as well. This is sometimes referred to as the 'wick effect' and has been shown to be a mechanism of transport for pesticides from water-saturated soils [18]. In this particular case the 'wick effect' is probably of less significance, since the average water evaporation rate was only 5.5×10^{-6} l cm^{-2} h^{-1} (see also Fig. 4). The porewater concentration of DBF is $w_A / K_{oc} f_{oc} = 0.05$ mg l^{-1}. Hence, the convective flux of DBF is 0.25 ng cm^{-2} h^{-1}, which is small compared

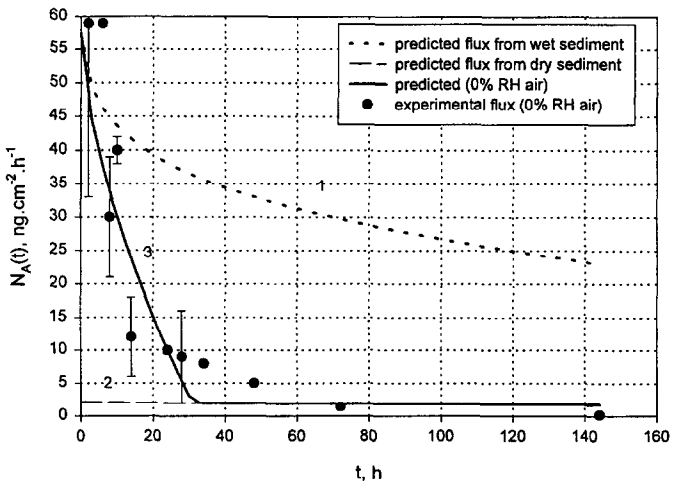

Fig. 4. Flux to air of DBF from Rouge River sediment. Dry air at 100 ml min^{-1} passed over wet sediment.

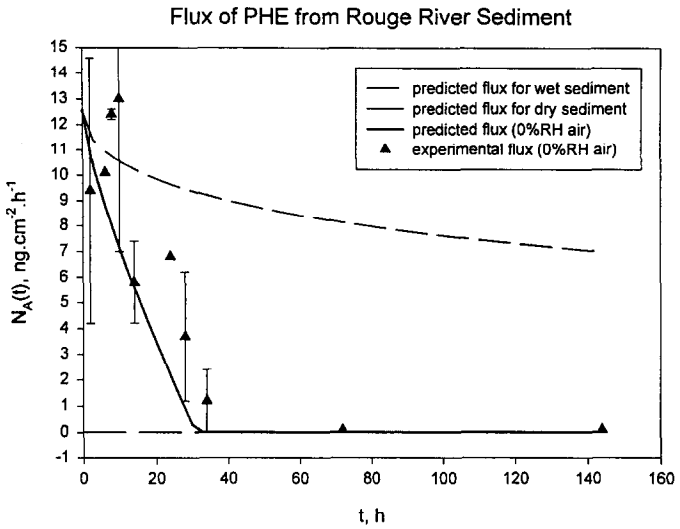

Fig. 5. Sediment-to-air flux of PHE from Rouge River sediment. Dry air at 100 ml min^{-1} passed over wet sediment.

to the observed initial flux. Furthermore, the 'wick' effect is only significant if a constant evaporation rate is maintained as a result of water continually flowing up and the entire surface is kept moist [24]. Neither of these conditions are met in this experiment. As both DBF and water are depleted from the surface and a 'dry' zone of sediment is formed, further mass transport of DBF from deeper 'wet' sediment layers occurs by diffusion. Since the 'dry' zone has a high sorptive capacity, further volatilization of DBF out of the sediment will be restricted and hence the flux will quickly attain a small value. Similar behavior was also noted for the flux of PHE and PYR from the sediment (Fig. 5 and Fig. 6). The initial flux ($t = 2$ h) for PHE was 10 ng cm^{-2} h^{-1} and for PYR was 0.7 ng cm^{-2} h^{-1}. The final steady state flux after 144 h was 0.11 ng cm^{-2} h^{-1} for PHE and 0.13 ng cm^{-2} h^{-1} for PYR. For PYR the flux was low and almost constant, indicating a smaller influence of the sediment-side diffusion process, i.e., a larger air-side resistance control on its flux, as suggested by theory. The relative magnitudes of the initial fluxes are in the order DBF > PHE > PYR and are consistent with the relative magnitudes of their Henry's constants. A mass balance on the organic compound in the microcosm can be done to assess the percent loss during the experiment. The mass lost in each interval of sampling can be obtained by multiplying the time step by the total area of the microcosms and the flux at the end of each time step. The integrated total mass of organic lost during the run, is $w_A W_s - \sum_i N_A(t_i) A(t_i - t_{i-1})$, where W_s is the total sediment mass in the microcosm. For the case of DBF presented in Fig. 5, the integrated mass of DBF lost in 144 h was 0.22 mg. Since 180 g of total sediment was used, the total mass of DBF initially in the microcosms was 7.2 mg. Thus, only 3.1% of the total mass of DBF was lost through volatilization in 6 days. Only 1.9% of PHE and 0.23% of PYR were lost during the same time period. The sharp decrease in flux with time was also observed in an earlier experiment on the volatiliza-

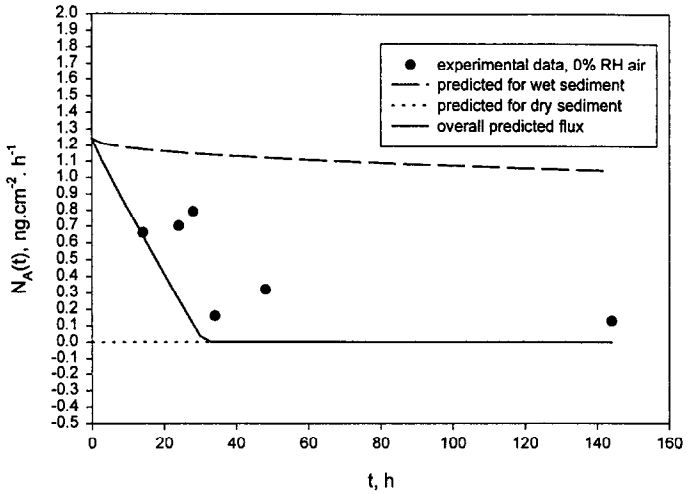

Fig. 6. Sediment-to-air flux of PYR from Rouge River sediment. Dry air at 100 ml min^{-1} passed over wet sediment.

tion of Aroclor 1242 (A-1242, a mixture of several congeners of polychlorinated biphenyls, PCBs) from a contaminated New Bedford harbor, MA sediment sample [8,19]. An earlier work by Igue et al. [30] also showed a similar behavior for the flux of a pesticide (dieldrin) from a 0.5 cm thick layer of a soil sample.

Fig. 4 also shows the predicted flux for DBF from the Rouge River sediment under different conditions. For the 'wet' sediment, the calculated value of R_{Fw} and D_e for DBF are respectively 1.68×10^5 and 0.018 cm^2 s^{-1}. These values for the 'wet' sediment were assumed to remain constant during one simulation. This implied no loss of moisture from the sediment and hence a constant value for R_{Fw}. The value of $k_a = 0.096$ cm s^{-1} for DBF was obtained from the boundary layer expression in Table 3 using $Re = 320$ and $Sc = 2.5$. Eq. (9) was also used for the 'dry' sediment conditions for which $\epsilon_w = 0$, $R_{Fd} = 4.42 \times 10^6$ and $D_e = 0.037$ cm^2 s^{-1}. These values were held constant throughout the second simulation, thus representing no change in R_{Fd}. The value of k_a used in this case was also 0.096 cm s^{-1}. For the 'wet' sediment with constant properties the initial flux predicted was comparable to the observed value while the flux at long times was larger than that observed in the experiments (curve 1 in Fig. 4). As expected, Eq. (9) predicted a much smaller flux for the 'dry' sediment with constant properties throughout the duration of the run (curve 2 in Fig. 4).

Table 3
Air-side mass transfer coefficient expressions

Theory	Expression
Penetration theory	$k_a = 2\sqrt{D_A v / \pi L}$
Boundary layer theory	$k_a = 0.677 Re^{1/2} Sc^{1/3} D_A / L$

Ref. [12].

In contrast to the predictions for sediments with constant properties, the experimental data showed a sharp decrease in flux that occurred in approximately 24 to 36 h. It is apparent from Fig. 4 that this steep decline in flux is indicative of a change in sediment conditions (from 'wet' to 'dry') as a result of water loss from the surface. Using the parameters from Table 2, the DBF flux predicted by Eq. (7) is indicated by the solid line (curve 3) in Fig. 4. The flux decreased from that of the wet sediment and remained constant at that for the dry sediment conditions after 31 h. As the drying progressed, the flux rapidly declined. The agreement between the predicted and experimental values of flux was satisfactory. The initial flux for DBF was predicted to be 57 ng cm^{-2} h^{-1}, while the experimental flux was observed to be 59 ± 26 ng cm^{-2} h^{-1}. Fig. 5 shows the simulation of the experimental data for PHE. Without any adjustable parameters the agreement with the experimental data for PHE also appeared to be quite satisfactory. Fig. 6 shows the experimental predicted flux for PYR. The predicted initial fluxes for PHE and PYR were 12 and 1.2 ng cm^{-2} h^{-1}, whereas the experimental values were 9.4 ± 5.2 and 0.66 ng cm^{-2} h^{-1}, respectively. In summary, it was apparent that in our experiments the initial flux was dependent on D_e/R_{fw} while the long term flux was a function of D_e/R_{Fd}. However, the intermediate flux was solely dependent on the dynamics of water evaporation from the sediment and the movement of the 'drying front' across the sediment surface in the direction of the air flow.

3.4. Effect of air-side mass transfer resistance on flux

Fig. 7 shows the effects of increasing air flow rate (velocity) on the sediment-to-air flux of DBF, PHE and PYR. The flux remained small at the low air flow rate (10 ml min^{-1}) that was maintained for 168 h. At that time the flow rate was increased to 100 ml min^{-1} and the flux dramatically increased. After 312 min, the flow rate was increased to 1000 ml min^{-1}, but no sudden increase in flux was noted. For example, in the case of DBF the flux remained at 2.0 ng cm^{-2} h^{-1} for 168 h at 10 ml min^{-1}, which then increased to an initial value of 59 ng cm^{-2} h^{-1} at 100 ml min^{-1} flow rate. At 100 ml min^{-1} flow rate, the flux decreased rapidly to a steady state value of 0.5 ng cm^{-2} h^{-1} after a total of 312 h of air flow. Increasing the flow rate further to 1000 ml min^{-1} showed no further discernible change in the flux which continued to remain at the steady state value (ca. 0.5 ng cm^{-2} h^{-1}). The effect of air flow rate (or air velocity) manifests itself through the equation for k_a (see Table 3). At small k_a values, the air-side resistance ($1/k_a$) dominates and hence the flux is small. At a higher air velocity, initially the process is controlled by the air-side resistance and a high flux will be noted, which as time progresses will get smaller as sediment-side diffusion takes over. For example, in the case of DBF, the magnitude of k_a from boundary layer theory is 0.031 cm s^{-1} and hence the predicted initial flux at 10 ml min^{-1} (velocity of 0.28 cm s^{-1}) is 18 ng cm^{-2} h^{-1}. Upon increasing the flow rate to 100 ml min^{-1}, the value of k_a increases to 0.096 cm s^{-1} and hence the predicted initial flux is 57 ng cm^{-2} h^{-1}. Thus, a 3-fold increase in initial flux of DBF is predicted as the air flow rate is increased 10 times. With increasing time the process becomes predominantly controlled by sediment-side diffusion. At such a stage further increase in the air flow rate (1000 ml min^{-1}) will not affect the flux since the term in k_a becomes less significant.

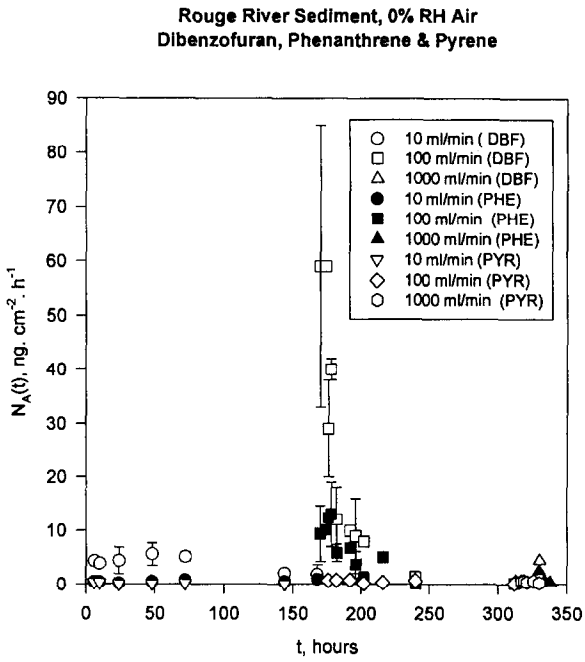

Fig. 7. Effects of different air flow rates on the flux to air of DBF, PHE and PYR from wet Rouge River sediment. Dry air (0% RH) used.

3.5. *Effect of air relative humidity change on flux*

Fig. 8 shows the effect of the air relative humidity change upon the flux of DBF. Fig. 9 shows the same data for PHE and PYR. The air flow rate over the wet sediment was

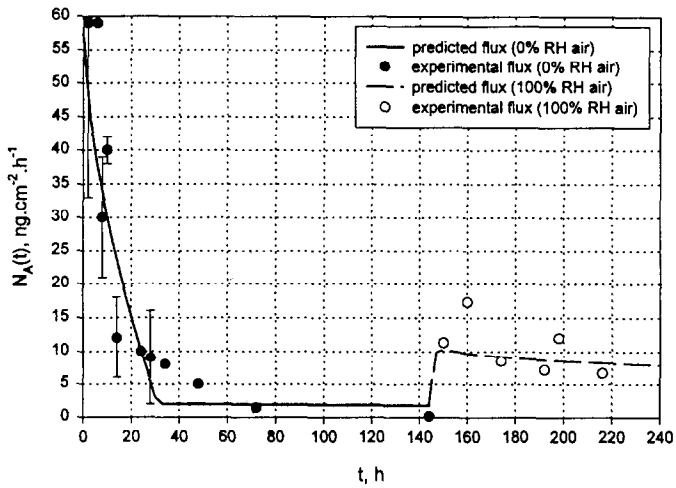

Fig. 8. Effects of different air relative humidities (0% and 100%) on the flux to air of DBF at 100 ml min^{-1} air flow rate.

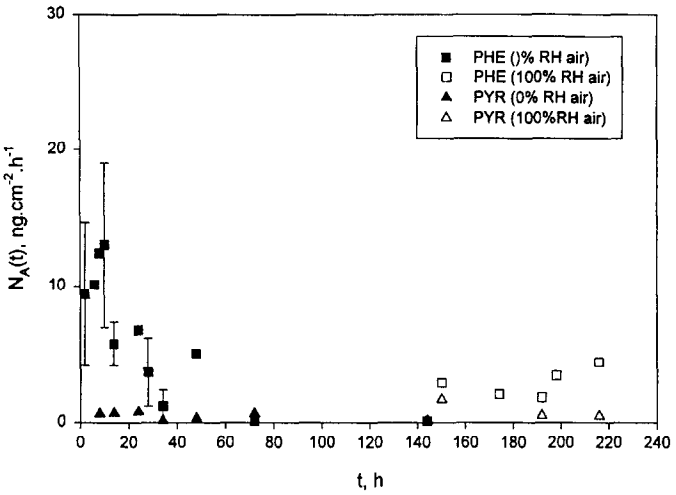

Fig. 9. Effects of different air relative humidities (0% and 100%) on the flux to air of PHE and PYR at 100 ml min^{-1} air flow rate.

maintained constant at 100 ml min^{-1} throughout the experiment. At the start of the experiment, air at zero relative humidity (dry air) was used. The initial flux of DBF was high (60 ng cm^{-2} h^{-1}) and quickly decreased to 0.2 ng cm^{-2} h^{-1} after 144 h of the experiment. At this point the air relative humidity was changed to 100% (humid air). An immediate increase in flux (ca. 32 ng cm^{-2} h^{-1}) was noticed, which subsequently decreased to a value of 8 ng cm^{-2} h^{-1} after 220 h of the experimental run. As discussed earlier (cf. Fig. 5), the flow of dry air quickly dries the surface layer, while at the same time increasing the capacity of the surface sediment layer. In the present case, the initial moisture of the sediment was measured to be 20% w/w, which decreased to 0.67% w/w after 72 h of contact with dry air, and increased to ca. 2% w/w after 6 days of contact with humidified air. When the surface is dry, there is very little competition for adsorption sites for organics on the sediment surface since the moisture content in the air is zero. Slow diffusion of organics from the deeper sediment layers occur in response to the existing concentration gradient, and the organics accumulate in the surface layer. As soon as the relative humidity in the air increases, the water molecules effectively displace the sorbed organics and their vapor concentration and consequently the flux to air increases. At 100% relative humidity, there is very little loss of moisture from the surface of the sediment, and despite this fact the chemical flux to the air is substantial. Therefore, it can be concluded that the loss of chemical from a moist sediment is not necessarily dependent on the loss of moisture from the surface. The steady state flux at 100% air RH remained higher (8 ng cm^{-2} h^{-1}) than the steady state flux when dry air was passed over a wet sediment (0.2 ng cm^{-2} h^{-1}). The initial flux upon changing to humid air did not reach that at the beginning of the run for the wet sediment using dry air, indicating that the sediment was only partially water-saturated with humid air. Further, since the final average moisture content of the sediment was ca. 2%, it was clear that the sediment did not resaturate as a result of contact with humid air. It is well

known that the equilibrium moisture content of porous solids depends on the direction in which equilibrium is approached [29]. A different value is obtained according to whether a wet sample is allowed to dry (desorption) or whether a dry sample is allowed to adsorb moisture (sorption). Hence, the sediment can be considered to go from 'dry' conditions after 144 h of contact with dry air to 'damp' conditions after an additional 144 h contact with humid air.

Fig. 8 also shows the predicted flux upon changing the air relative humidity. For this case, a 'damp front' was considered to move across the sediment upon changing the air relative humidity to 100%. This suggested that R_F changed from that of a 'dry' sediment (R_{Fd}) to that of the intermediate 'damp' sediment (R_{Fp}). Note that R_{Fp} is larger than for the 'wet' sediment, R_{Fw}. The time (τ_{damp}) that it took for the 'damp front' to move across the sediment is scaled in proportion to the final moisture content. Thus, $\tau_{damp} = \tau_{evap}\gamma_f/\gamma_0$, where γ_f is the final moisture content (g g^{-1}) at the end of the experiment with humid air. For the present case, τ_{damp} was estimated to be 3.2 h. For the case of the advancing 'damp front' the overall flux of the contaminant was calculated using the following equation:

$$N_A(t) = N_{Ap}(t)\frac{t}{\tau_{damp}} + N_{Ad}(t)\left(1 - \frac{t}{\tau_{damp}}\right) \tag{12}$$

where $N_{Ap}(t)$ is the flux from the 'damp' sediment calculated using Eq. (9) where R_{Fp} and K^*_{dp} are used. A value of $K^*_{dp} = 1.2 \times 10^6$ cm^3 g^{-1} was estimated using the relationship $K^*_{dp} = K^*_{dd}(1 - \gamma_f/\gamma^m_w)$ as suggested by Valsaraj [11]. The value of $\gamma^m_w = 0.026$ g g^{-1}, the monolayer capacity of the sediment for water was calculated in a manner identical to that described earlier for the contaminant using the equation $0.917fS_a(d^2_w M_w/N)^{1/3}$. The value of R_{Fp} so calculated was 8.5×10^5. Fig. 10 shows the predicted flux for DBF. It increased to a maximum of 10.1 ng cm^{-2} h^{-1} in approximately 3 h and declined slowly to 7.3 ng cm^{-2} h^{-1} in 144 h. There are no adjustable parameters in this simulation, and the model is completely predictive. We observed fair agreement with the experimental data.

A long term experiment (28 days) was conducted to observe the effects of cyclic air relative humidity changes on the flux of DBF. The results of that experiment are displayed in Fig. 10. The air flow rate was maintained at 100 ml min^{-1} throughout the duration. Initially, a wet sediment sample was placed in the microcosm and dry air was passed over it for seven days. Subsequently, the air relative humidity was changed to 100% and the flux measured for 7 days as in the previous experiments. Thereupon, the air relative humidity was changed to 0% and the experiment continued for 7 more days. Finally, a switch to humid air was made for the last seven days of the experiment. During the first seven days of the run, the DBF flux decreased rather rapidly from a value of 27 ng cm^{-2} h^{-1} at 6 h to a final value of 0.01 ng cm^{-2} h^{-1} after 7 days. This is in line with the observations we discussed earlier for the case of dry air over the wet sediment. When switched to humid air over this sediment, the flux increased to 12 ng cm^{-2} h^{-1} in 30 h (cumulative time, $t = 198$ h) and subsequently decreased slowly to 1.7 ng cm^{-2} h^{-1} after 7 days ($t = 342$ h). Thus, the long-term flux with dry air was significantly lower than that with humid air. At $t = 342$ h, the air was changed back to

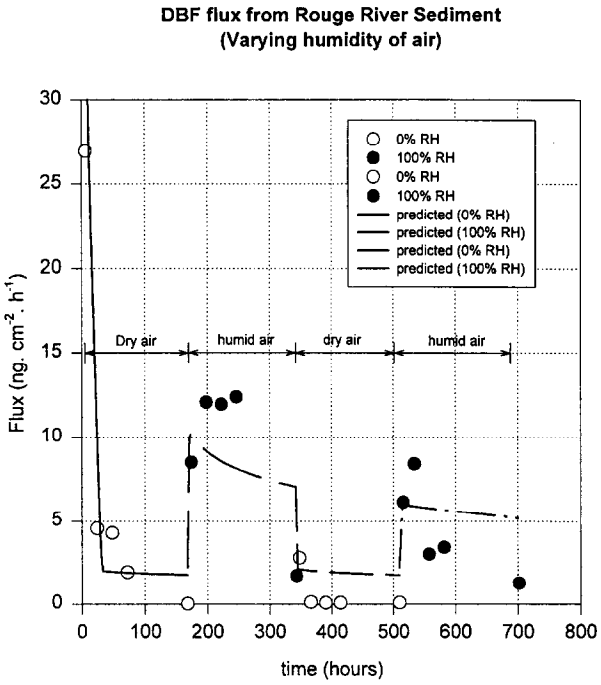

Fig. 10. Effects of cyclic changes in air relative humidity (0% and 100%) in a long-term experiment conducted for 28 days.

dry conditions; the flux decreased quickly to 0.08 ng cm^{-2} h^{-1} after 7 days ($t = 510$ h). Further, when the air was switched back to 100% RH, the flux quickly increased to 6.1 ng cm^{-2} h^{-1} and decreased to a value of 1.3 ng cm^{-2} h^{-1} after 7 days ($t = 702$ h). If one discards the low value at 346 h in the first cycle, it appears that the profile in the second cycle was an extrapolation of the first, indicating that the sediment had reached its 'damp' region in both cases as soon as contact of dry sediment with humid air occurred. The rate of decline in flux was much slower with humid air than with dry air. The final steady state flux with humid air was distinctly larger than it was with dry air. Indeed as we suggested earlier, the water molecules in the air effectively displaced DBF from the sediment surface and hence increased the flux during the change to humid air. Also shown in Fig. 10 is the predicted flux using the models described earlier. The trend in the predicted flux matched that in the experiment, although the agreement for the dry sediment was only marginal. The predicted values of flux were distinctly large when the air was humid. The predicted flux from the second cycle using humid air was found to be an extrapolation of that from the first cycle, while the same held true also for the flux during the first and second cycles using dry air.

The fact that purely predictive models gave results that were within the range of the experimental data lends credibility to the assumed mechanisms of air emissions in the models. For the most part, it appears that the effects of water evaporation upon the air emissions of PAHs from freshly exposed thin sediment layers that form the basis of the

model are substantially correct. There are, however, several limitations to the experiments and the model reported in this work. The experiments reported herein are on thin sediment layers and are only representative of field conditions in the upper few centimeters of sediment layers. The scale of the experimental microcosm, viz., a thin sediment layer and a small cross-sectional area, was such that the end-effects appear to play a dominant role in the manner in which drying proceeds. Changes in relative humidity in the natural atmosphere will occur more frequently, perhaps a few hours or so. Wind directions and velocity will also change rapidly. Therefore, in the field the formation and movement of a 'drying front' as seen in these small lab-scale experiments are unlikely. The drying of field sediments will create vertical profiles in sediment moisture content. The flux from deep sediments such as occur in actual field conditions, will then be dependent on (i) the variation in sediment moisture content in the vertical direction with time and, (ii) the corresponding change in K_d^* or R_F with moisture content within the sediment. Neither of these factors have been adequately studied at the present time. The additional features necessitate a refined model, one that invokes a slowly developing dry surface sediment zone overlying the wet sediment. The continuous loss of moisture from a 'wet' sediment will eventually produce visible cracks which can persist throughout the sediment depth and influence the flux to air. The present theoretical framework does not include this effect. The above shortcomings await further experiments using deeper sediment microcosms, more frequent relative humidity changes, and an appropriate mathematical formulation of the problem which are all being currently pursued and will be reported in a subsequent paper. It has been recently reported that PAHs (anthracene, phenanthrene and pyrene) undergo oligomerization to higher molecular weight aromatic products on clay mineral surfaces under dry conditions [22]. This reaction was retarded on moist surfaces due to inhibition by adsorbed water molecules. This adds an extra level of complexity to the modelling of air emission flux from sediments.

4. Conclusions

It has been demonstrated in laboratory microcosms that the exposed Rouge River sediment can be a source of semi-volatile organics to the air. The rate of volatilization was controlled by both the air-side boundary layer resistance and the sediment-side diffusion resistance. Higher air velocity made the volatilization a sediment-side controlled process. The flux was dependent on the sediment–air partition coefficient and the sediment loading of the chemical. It was also a strong function of the air relative humidity. Flow of dry air (0% RH) over a wet sediment quickly depleted the water and organics from the surface. The dry surface sediment restricted movement of the organics due to its high sorptive capacity. Upon remoistening the sediment using humid air (100% RH) the sorbed organics were released to the air. This process can be of significance in the natural environment where contaminated sediments go through cyclic wet and dry periods in a CDF.

Over the long term the transport of semi-volatile organic compounds from a contaminated sediment or dredged material to air is rate limited by molecular diffusion

of chemical through the pore spaces within the sediment. The sediment particles with their moisture covering are the chemical sources, always maintaining an equilibrium concentration in the pore spaces. Water movement due to wet–dry cycles will likely have a secondary effect on the contaminant loss rate from the upper soil layers. In general, the effect will be to enhance the rate. Wet and dry cycles will cause the contaminant to move upward in clay and low-permeability sediments. Water evaporation at the surface and its capillary rise transport the soluble chemicals upward. Here it readsorbs onto cleaner surface sediment and awaits dry-out so it can reevaporate. In sandy, low-permeability sediments, downward leaching is likely to occur.

Soil surface cracking will also likely influence the contaminant loss rates. Cracking may change the overall sediment porosity and modify the diffusion pathway to the surface. Evaluation of this and other secondary effects on the emission rate in the upper sediment layers await further development of mathematical models and long-term experiments on deep sediments in microcosms and also in the field. These aspects are currently being pursued in our laboratory and will be reported later.

5. List of notations

A_T Total area of the sediment–air interface (cm^2).
$A_d(t)$ Area of the 'dry' sediment zone at any time t (cm^2).
$A_w(t)$ Area of the wet sediment zone at any time t (cm^2).
B_A BET isotherm parameter for the contaminant.
C_a Air phase pollutant concentration (ng cm^{-3}).
d_A Density of pollutant (g cm^{-3}).
d_w Density of water (g cm^{-3}).
D_e Effective diffusivity of pollutant in sediment (cm^2 h^{-1}).
D_A Air diffusivity of pollutant (cm^2 h^{-1}).
f Packing factor.
f_{oc} Fraction of organic carbon in the sediment.
g Gravitational constant (cm s^{-2}).
H Depth of sediment in the microcosm (cm).
H_c Henry's constant (molar ratio) for the contaminant.
k_a Air-side mass transfer coefficient (cm h^{-1}).
K^*_{dd} Dry sediment–air partition constant for pollutant (cm^3 g^{-1}).
K^*_{dw} Wet sediment–air partition constant for pollutant (cm^3 g^{-1}).
K^*_{dp} Damp sediment–air partition constant for pollutant (cm^3 g^{-1}).
K_{oc} Organic carbon-based sediment–water partition constant (cm^3 g^{-1}).
L Length of the sediment–air interface in the air flow direction (cm).
$N_A(t)$ Average flux of solute from sediment to air (ng cm^{-2} h^{-1}).

$N_{Ad}(t)$ Flux from the dry sediment to air (ng cm^{-2} h^{-1}).
$N_{Aw}(t)$ Flux from the wet sediment to air (ng cm^{-2} h^{-1}).
$N_{Ap}(t)$ Flux from the damp sediment to air (ng cm^{-2} h^{-1}).
p^0_w Saturation pressure of water at temperature T (atm).

q Air flow rate over the sediment surface ($cm^3\ h^{-1}$).
R_{Fd} Retardation factor for solute in dry sediment.
R_{Fp} Retardation factor for solute in damp sediment.
R_{Fw} Retardation factor for solute in wet sediment.
Re Reynolds number ($= vL/\nu_a$).
Sc Schmidt number ($= \nu_a/D_A$).
ν_a Kinematic viscosity of air ($cm^2\ h^{-1}$).
v Velocity across the sediment surface ($cm\ h^{-1}$).
w_A^0 Initial sediment concentration of contaminant A ($ng\ g^{-1}$).
w_s Total sediment mass (g).

Acknowledgements

This research was supported by a grant (R819165-01) from the US EPA through the Hazardous Substances Research Center (South and Southwest) at LSU. It has not been subject to the required EPA peer review and hence does not necessarily reflect the views of the US EPA. At the US Army Engineer Waterways Experiment Station, the work was supported by the Long-Term Effects of Dredging Operations (LEDO) program.

References

[1] K.T. Valsaraj, L.J. Thibodeaux and D.D. Reible, ASTM STP 1293 (1995) 227.
[2] K.T. Valsaraj and L.J. Thibodeaux, J. Haz. Mater. 19 (1988) 79.
[3] W.F. Spencer, T.D. Shoup, M.M. Cliath, W.J. Farmer and R. Haque, J. Agric. Food. Chem. 27 (1979) 273.
[4] L.W. Lion, S.K. Ong, S.R. Linder, J.L. Swanger, S.J. Schwager and T.B. Culver, Sorption Equilibria of Vapor Phase Organic Pollutants on Unsaturated Soils and Soil Minerals, Final Report to the Environics Divison, Air Force Engineering and Services Center, Tyndall Air Force Base, FL, Report No. ESL-TR-90-05 (1990).
[5] L.W. Peterson, P. Moldrup, Y.H. El-Farhan, O.H. Jacobsen, T. Yamaguchi and D.E. Rolson, J. Environ. Qual. 24 (1995) 725.
[6] C.T. Chiou and T.D. Shoup, Environ. Sci. Technol. 19 (1985) 1196.
[7] C.T. Erkey, J.F. Campagnolo and A. Akgerman, Sep. Purif. Meth. 24 (1995) 129.
[8] J.M. Brannon, Laboratory Assessment of Volatilization from New Bedford Harbor Sediment, Memorandum for Record, US Army Engineer Waterways Experiment Station, Vickburg, MS, WESES-A (1989).
[9] L.J. Thibodeaux, Theoretical Models for Volatile Emissions from Dredged Materials — Comparison of Predicted and Laboratory Measurements for New Bedford Harbor Sediment, Memorandum for Record, US Army Engineer Waterways Experiment Station, Vicksburg, MS, Contract No. DACW39-89-M-0207 (1989).
[10] L.J. Thibodeaux, Environmental Chemodynamics, 2nd Edn. (Wiley, New York, 1996).
[11] K.T. Valsaraj, Elements of Environmental Engineering- Thermodynamics and Kinetics (CRC Press/Lewis, Boca Raton, FL, 1995).
[12] L.J. Thibodeaux and H.D. Scott, In: W.B. Neely and G.E. Blau (Eds.), Environmental Exposure from Chemicals, Vol. I (CRC Press, Boca Raton, FL, 1985) pp. 65–89.
[13] U.S. EPA, Test Methods for Evaluating Solid Waste- Physical and Chemical Methods, SW-846, 2nd Edn., NTIS, Springfield, VA, NTIS No. PB87-120291 (1982).

[14] G.J. Thoma, Studies on the Diffusive Transport of Hydrophobic Organic Chemicals in Bed Sediments, Ph.D. Thesis, Louisiana State University, Baton Rouge, LA (1994).
[15] S. Batterman, I. Padmanabhan and P. Milne, Environ. Sci. Technol. 30 (1996) 779.
[16] T. Luong, The Mobility and Partitioning of PAHs in Oil and Grease Contaminated Sediments, M.Sc. Thesis, Louisiana State University, Baton Rouge, LA (1996).
[17] R.R. Dupont, Environ. Prog. 5 (1986) 199.
[18] W.F. Spencer and M.M. Cliath, J. Environ. Qual. 5 (1973) 279.
[19] L.J. Thibodeaux, K.T. Valsaraj, D.D. Reible and J.M. Brannon, In: Proc. of the 21st Annu. RREL Res. Symp., US EPA, Cincinnati, OH, Document No. EPA/600/R-95/012 (1995) 232–235.
[20] J.H. Montgomery, Groundwater Chemicals Desk Reference, 2nd Edn. (CRC Press, Boca Raton, FL, 1996).
[21] M.R. Palermo and J. Miller, Disposal Alternatives for PCB-Contaminated Sediments from Indiana Harbor, Indiana, Miscellaneous Paper EL-87-9, Volume I, US Army Engineer Waterways Experiment Station, Vicksburg, MS (1987).
[22] S.K. Lotfabad, M.A. Pickard and M.R. Gray, Environ. Sci. Technol. 30 (1996) 1145.
[23] H.S. Carslaw and J.C. Jaeger, Conduction of Heat in Solids, 2nd Ed. (Oxford University Press, Oxford, 1959).
[24] R.G. Thomas, in: W.J. Lyman, W.F. Reehl and D.H. Rosenblatt (Eds.), Handbook of Chemical Property Estimation Methods (American Chemical Society, Washington, D.C., 1990) pp. 16-1 to 16-50.
[25] M.N. Özişik, Heat Conduction, 2nd Edn. (Wiley, New York, 1993).
[26] D.R. Shonnard, R.L. Bell and A.P. Jackman, Environ. Sci. Technol. 27 (1994) 457.
[27] K.T. Valsaraj and L.J. Thibodeaux, In: J.L. Schnoor (Ed.), Fate of Pesticides and Chemicals in the Environment (Wiley, New York, 1992) Ch. 10, pp. 155–175.
[28] R.J. Millington and J.M. Quirk, Trans. Faraday. Soc. 57 (1961) 1200.
[29] W.L. Badger and J.T. Banchero, Drying, Introduction to Chemical Engineering (McGraw-Hill, Singapore, 1955) Ch. 10, pp. 469–520.
[30] K. Igue, W.J. Farmer, W.F. Spencer and J.P. Martin, Soil Sci. Soc. Amer. Proc. 36 (1972) 447.